Tumor Biol. (2014) 35:12205–12215
DOI 10.1007/s13277-014-2529-1

RESEARCH ARTICLE

Tumor vascular homing endgolin-targeted radioimmunotherapy in hepatocellular carcinoma

Chong-Ling Duan · Gui-Hua Hou · Yan-Ping Liu · Ting Liang · Jing Song · Jian-Kui Han · Chao Zhang

Received: 20 July 2014 / Accepted: 20 August 2014 / Published online: 28 August 2014

Abstract Endoglin is a proliferation-associated cell membrane antigen and overexpressed in the angiogenic vasculature of solid tumors. However, the applications of endoglin (ENG)-targeted radioimmunotheray in hepatocellular carcinoma have not been reported yet. Therefore, the aim of this study was the visualization of both the development of hepatocellular carcinoma (HCC) tumor burden and therapeutic effect with ENG-targeted ^{131}I-anti-ENG mAb (A8), via in vivo noninvasive fluorescence imaging (NIFLI) of SMMC7721-green fluorescent protein (GFP) cells. A8 showed a dose-dependent, time-dependent suppression on the proliferation of SMMC7721-GFP cells and human umbilical vein endothelial cells (HUVECs) in vitro. Tube formation assay showed that ^{131}I-A8 markedly inhibits HUVECs to form extensive and enclosed tube networks. The results showed that the radiochemical purity of ^{131}I-A8 was 92.8 % and ^{131}I-A8 maintained more stable in serum than in saline and had high affinity against SMMC7721-GFP cells. The pharmacokinetics of ^{131}I-A8 was in accordance with the two-compartment model, with a rapid distribution phase and a slow decline phase. NIFLI exhibited a good relation between the fluorescent signal and tumor volume in vivo. Furthermore, treatment with ^{131}I-A8 resulted in significant tumor-growth suppression on the basis of the reducing fluorescent signal and a remarkably decreased tumor weight in treated animals. These results were further verified by RT-PCR and immunohistochemistry staining. Our findings indicate that ^{131}I-A8 can be used as ENG-targeted therapy for hepatocellular carcinoma, and noninvasive fluorescence imaging provides valuable information on tumor burden and effectiveness of therapy.

Keywords Endgolin · Hepatocellular carcinoma · Radioimmunotherapy · Noninvasive fluorescence imaging

Introduction

Hepatocellular carcinoma (HCC) is the most common form of primary liver cancer and the third most deadly malignancy worldwide, particularly in China where the mortality rate associated with HCC accounts for more than 50 % of the worldwide rate [1]. Although advancing in diagnosis, modalities, and surgical techniques [2–4], the long-term prognosis of patients with HCC remains poor, mainly because of frequent recurrence and metastasis after curative resection [5–7]. Therefore, an effective and alternative treatment strategy is urgently needed.

Angiogenesis-targeted therapy is a promising strategy for cancer therapy. It can be more effective for destroying established tumors than conventional antiangiogenic therapy [8]. Thus, a critical issue in angiogenesis-targeted therapy is availability of an appropriate target. In this concept, endoglin (ENG) is a cell membrane glycoprotein representing a prime vascular target to implement innovative antibody-based diagnostic and therapeutic strategies according to emerging in vitro and in vivo preclinical evidence. It is a component of the receptor complex of transforming growth factor (TGF-β), a pleiotropic cytokine involved in cellular proliferation, differentiation, and migration. It is present on endothelial cells of both peri-tumoral and intratumoral blood vessels and on tumor stromal components [9, 10]. Recently, several studies indicated that ENG represents a more specific and sensitive marker for tumor angiogenesis and/or tumor progression than the commonly used pan-endothelial markers

C.-L. Duan · G.-H. Hou · Y.-P. Liu · T. Liang · J. Song · J.-K. Han · C. Zhang (✉)
Key Laboratory for Experimental Teratology of the Ministry of Education and Institute of Experimental Nuclear Medicine, School of Medicine, Shandong University, Jinan, China
e-mail: sd2012zhang@126.com

such as CD34 and CD31 in various types of human malignancies [11, 12]. In HCC, staining for ENG was reported to be strong at the areas of active angiogenesis including tumor edge, while it was less intense in the central area of the tumor and not detectable in the adjacent normal tissue [13].

Radioimmunotherapy is a therapeutic modality which delivers alpha, beta, or gamma emitters directly to targeted cancer cells. It has the advantage of regressing tumors while reducing nontargeted toxicities with the help of neutralizing antibodies. The effective use of radioimmunotherapy for cancer treatment is closely linked to the optimal application of imaging for staging and tumor characterization. Therefore, any improvement in the field of imaging will impact on radiation oncology per se. Noninvasive fluorescence imaging (NIFLI) using genetically encoded fluorescence proteins (FP) is a promising tool to detect and monitor primary tumor growth as well as metastatic disease and their therapy response in vivo. Even simultaneous imaging of separated fluorophores reporting different model parts or processes, e.g., therapeutic agent, drug carrier system, and therapy target, is possible [14, 15].

In this study, by labeling anti-ENG monoclonal antibody (mAb) with ^{131}I, we acquired a radioactive tumor targeting drug ^{131}I-anti-ENG mAb and investigate its in vitro stability, binding affinity, in vivo pharmacokinetics, and tumor localization behavior. In addition, the radioimmunotherapy effect of ^{131}I-anti-ENG mAb on SMMC7721-green fluorescent protein (GFP)-derived tumor was monitored by NIFLI.

Materials and methods

Cell culture

Human HCC cell line SMMC7721-GFP stably expresses GFP at high levels, and human normal liver cell line L-02 was obtained from the Cell Bank of Shanghai Institute for Biological Sciences (Shanghai, China). The cell lines were cultured in DMEM (Invitrogen, Carlsbad, CA), all supplemented with 100 U/ml penicillin (Gibco BRL, Gaithersburg, MD), 100 U/ml streptomycin (Gibco BRL), and 10 % fetal bovine serum (Gibco BRL). Human umbilical vein endothelial cells (HUVECs) were stored in my laboratory and grown in endothelial cell growth medium (ScienCell Research Laboratories). Cells grew by attaching to the wall in a monolayer, and the cells in the logarithmic growth phase were used for experiments. After the cells covered the entire culture bottle bottom, digestion and passage were conducted with 0.25 % pancreatin under aseptic conditions. All cells were cultured in a humidified atmosphere with 5 % CO_2 at 37 °C. Cells were regularly passaged to maintain exponential growth.

Animal model

The HCC tumor models were established by subcutaneous injection of 5×10^6/200 μl SMMC7721-GFP cells into the right upper back of male BAlB/cA-nu mice (20–25 g, 5–8 weeks, Animal Center of Peking University). Mice were maintained in a protected environment in a laminar flow unit and given sterilized food and water ad libitum. All animal studies were conducted under a protocol approved by the School of Medicine, Shandong University Institutional Animal Care and Use Committee.

Cell proliferation assay

The effect of the inhibition of the anti-ENG mAb (A8, Santa Cruz Biotechnology, Europe) on the proliferation of SMMC7721-GFP, HUVECs cell lines were examined using CCK-8 kit (boster Co. China) according to the manufacturer's instructions. After cells in the logarithmic growth phase were digested and collected and prepared into a cell suspension with a concentration of 3×10^4/ml, cell suspension was inoculated into four 96-well plates (100 μl/well).The four 96-well plates respectively represent four different time points: 12, 24, 48, and 72 h. In each 96-well plate, the cell suspension was divided into six groups (the control group and A8 5, 10, 20, 40, and 60 μg/ml group). In addition, the blank group (only full culture medium, without cells) was set, and the blank was used for zero calibration during colorimetric determination. The cells were incubated in the incubator containing 5 % CO_2 at 37 °C at a saturated humidity respectively for 12, 24, 48, and 72 h. At 1 h before culture completion, CCK-8 (10 μl) was added into each well, and the cells were continuously cultured at 37 °C for 1 h. The optical density (OD) was then read at 450 nm using a microplate reader. The experiment was conducted in triplicate. The cellular proliferation inhibition ratio was calculated according to the following formulas: Inhibition ratio (%)=[1−(OD value of the test group/OD value of the control group)]×100.

Targeting ability study of ^{131}I-A8

Radioiodination of A8 radiochemical stability and pharmacokinetic analysis

Two hundred forty micrograms A8 was iodinated with 50 μl Na^{131}I (185 MBq) (China Institute of Atomic Energy, Beijing, China) using the iodogen method as described previously [16]. Radioiodinated A8 was separated from free iodine using size exclusion columns (Sephadex G-25, Amersham Pharmacia Biotech, Uppsala, Sweden). Radiochemical purity was determined by paper chromatographic method using strips on two-paper sheet (1 cm width and 13 cm length) as described [17, 18] with modifications. Radiochemical purities

were measured at 1, 6, 12, 24, 48, and 72 h, respectively, to assess the stability. Ten percent potassium iodide was added to mice drinking water 3 days before injection of ^{131}I-labeled antibody to block the thyroid gland. 0.37 MBq ^{131}I-A8 was injected into the tumor burden mice through the tail vein. Pharmacokinetic analysis was conducted as follows: 10-μl blood samples were taken from periorbital vein of four mice at different times after injection of ^{131}I-A8 and then the radioactivity was measured by γ scintillation counter. The distribution half-life ($T_{1/2\alpha}$), the elimination half-life ($T_{1/2\beta}$), and mean residence time (MRT) were calculated.

Cellular radioligand-based binding assay

The radioligand-based binding assay was carried out in borosilicate glass tubes as described [19, 20] with modifications. For saturation studies, the reaction mixture contained 200-μl SMMC7721-GFP cells (5×10^6/ml and 100 μl ^{131}I-A8 (0.01–50 nM, diluted in 1× PBS) in a final volume of 500 μl. 0.1–1,000 nM unlabeled A8 and 10 nM ^{131}I-A8 were used for competition binding assay. The mixture was incubated at 37 °C for 2 h. The bound radioligand was separated by rapid vacuum filtration through Whatman GF/B filters using a cell harvester followed by 3×2 ml washes of PBS at room temperature. The radioactivity of filters containing the bound radioligand was assayed in test tube by Wipe Test/Well Counter (Caprac; Capintec, Ramsey, NJ). The equilibrium dissociation constant (K_D), the maximum number of binding sites (B_{max}), the inhibitor constant (K_i), and the half maximal inhibitory concentration (IC_{50}) were calculated.

Tube formation assay

The ability of endothelial cells to sprout new blood vessels suppressed by ^{131}I-A8 was examined in HUVECs angiogenesis in vitro model [21]. Briefly, 5×10^4 HUVECs were collected, resuspended in a conditioned medium which contain different dose of antibody, seeded in 24-well plates that were coated with 100 μl of gelled matrigel (BD Biosciences, USA), and cultured in a humidified 37 °C, 5 % CO_2 incubator. After incubation from 0.5 to 8 h, numbers of branching points were counted. The data were obtained from triplicate wells under each experimental condition at each time point. Photographs from randomly chosen fields were taken using a digital camera when cords were formed.

Radioimmunotherapy of ^{131}I-A8 on tumor-bearing mice

The subcutaneous tumor-bearing mice were randomly divided into the experimental group and control group (n=8). When the volume (volume=(length×width^2)/2) [22] of the tumors) increased 50 mm^3, they were given intratumorally injections with 3.7 MBq ^{131}I-A8 (0.5 μg/g) or control phosphate-buffered saline (PBS) in 0.1 ml. The mAb dose was chosen based on the dose-dependent titration experiment [23]. The treatment was administered intratumorally once a week for a month. At the end of the experiment, tumor tissue from each animal was excised and then weighed. The inhibition rate was calculated using the formula inhibition rate=$[(\text{weight}_{\text{control group}}-\text{weight}_{\text{experimental group}})/\text{weight}_{\text{control group}}]\times100$ %.

NIFLI to monitor the treatment efficacy

In vivo GFP images were obtained using the in vivo FPRO imaging system, using the appropriate filters (excitation=445–490 nm, emission=535 nm). The parameters of CCD were fov=80–100, binning=2×2, and exposure time=5 sec. At the end of the imaging period, a grayscale reference image was collected under white light (excitation=445–490 nm, emission=0, fov=80–100, binning=0, exposure time=0.175 sec). Activity was quantified by viewing the region of interest (ROI) in the tumor analysis software molecular imaging standard edition (MISE) that is supplied with the Carestream. Fluorescence images and grayscale reference images were fused together with MISE. The signal intensities from manually derived regions of interest were expressed as photon flux (counts/s). The fluorescent signals are presented in color: blue for the lowest and red for the highest intensity.

RT-PCR

The expression of ENG mRNA was evaluated by reverse transcription polymerase chain reaction (RT-PCR). Total RNA was extracted from the cell lines or freshly isolated tumor and normal liver tissue by use of TRIzol reagent (Invitrogen, Carlsbad, CA). Oligo (dT)-primed complementary DNA (cDNA) synthesis involved use of Superscript™ III reverse transcriptase (Invitrogen). Transcripts were amplified from reverse-transcribed cDNA by use of SYBR Green (Invitrogen). The primer for ENG was chosen in cDNA portions by accessing human sequences in GenBank. The sequences were as follows: ENG forward 5′-GTGCTTCTGG TCCTCAGTGTA-3′ and reverse 5′-AGTTCCACCTTCAC CGTCAC-3′; GAPDH forward 5′-AGAAGGCTGGGGCT CATTTG-3′ and reverse 5′-AGGGGCCATCCACAGTCT TC-3′. Cycling conditions for amplification were as follows: denaturation step at 94 °C, followed by 35 cycles of 30 s at 94 °C, 1 min at 62 °C, and 1 s at 72 °C. PCR products were analyzed on 1.5 % agarose gels and stained with ethidium bromide. All the experiments were performed in duplicate,

and they were repeated at least three times. The relative expression of genes was analyzed using the $2^{-\Delta\Delta Ct}$ method.

Histological and immunohistochemical analyses

HCC tissues (freshly isolated tumor of the mice treated with PBS or ^{131}I-A8) and normal liver tissues were fixed in phosphate-buffered 4 % paraformaldehyde, embedded in paraffin, and cut into 4 μm thick sections. Sections were deparaffinized and stained with hematoxylin and eosin using a standard protocol to determine morphology. ENG protein expression was determined by immunostaining with A8 (1:200) using the streptavidin-biotin method. The sections were microscopically examined, and the positively stained fields were observed. At least ten fields per each section were observed. Image-Pro Plus v5.0.2 (Media Cybernetics, Inc., Bethesda, MD) was used for quantitative assessment of relative ENG protein expression levels.

Statistical analysis

SPSS v11.5 (SPSS Inc., Chicago, IL) was used for statistical analysis. Continuous data were expressed as mean±SD and compared by one-way ANOVA, followed by unpaired *t* test or paired *t* test as appropriate. The Pearson's correlation coefficient *r* was determined to assess the degree of correlation. A *P* value <0.05 was considered statistically significant.

Results

Cell proliferation assay

To assess the conceivable effects of anti-ENG mAb (A8) on both HUVECs and SMMC7721-GFP cells proliferation and survival, the number of viable cells at different times in vitro was measured with CCK-8 assays. SMMC7721-GFP cells

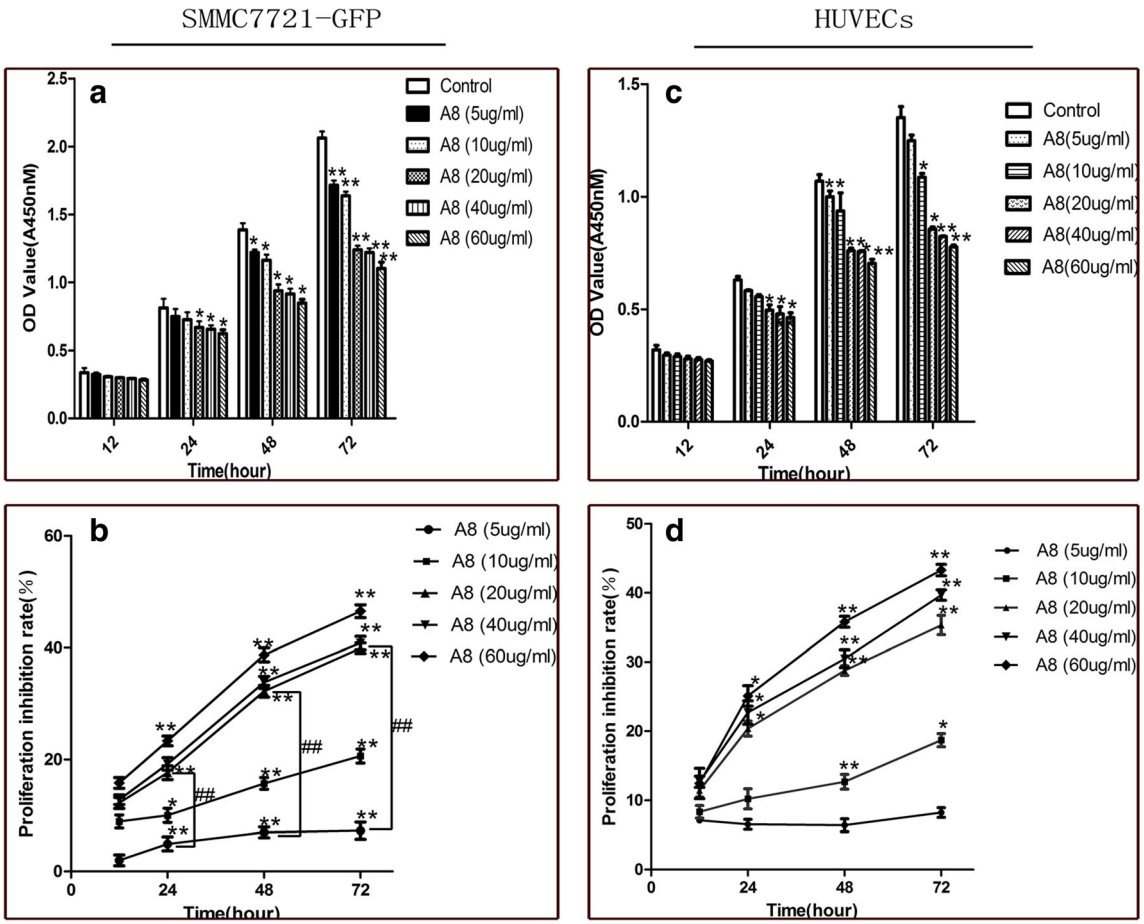

Fig. 1 The effect of A8 (anti-ENG mAb) on the proliferation of both SMMC7721-GFP and HUVECs cells. **a**–**b** SMMC7721-GFP cells were cultured with A8 (0, 5, 10, 20, 40, and 60 μg/ml, respectively) for 12, 24, 48, and 72 h (**a** **P*<0.05 and ***P*<0.01 vs. control; **b** **P*<0.05 and ***P*<0.01 vs. 12 h; #*P*<0.05 and ##*P*<0.01 vs. the same time-point in the 5 μg/ml group). **c**–**d** HUVECs were incubated with different concentrations of A8 for 12, 24, 48, and 72 h. The HUVECs proliferation inhibition rate was calculated after incubated with A8 (0, 5, 10, 20, 40, and 60 μg/ml, respectively). **c** **P*<0.05 compared with control; **d** **P*<0.05 and ***P*<0.01 vs. 12 h). Each point represents the mean of three independent experiments

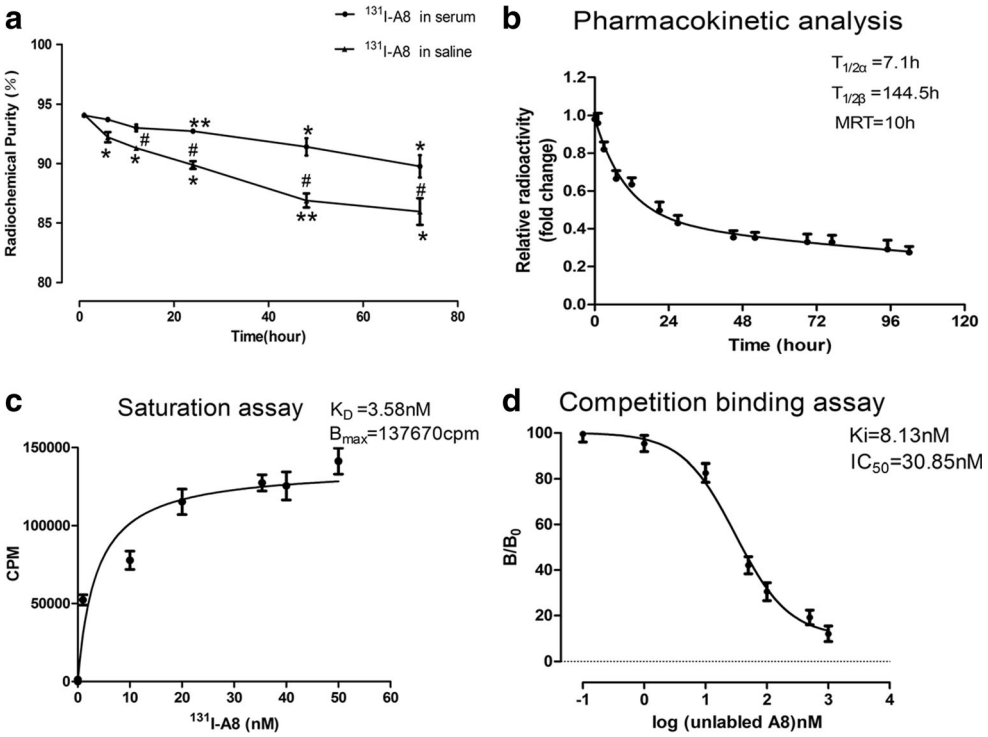

Fig. 2 ^{131}I-A8 was successfully radioiodinated. **a** The radiochemical purity of ^{131}I-A8. (*P<0.05 and **P<0.01 vs. 1 h; #P<0.05 vs. the same time-point in serum). **b** The pharmacokinetics analysis of ^{131}I-A8. $T_{1/2\alpha}$ distribution half-life, $T_{1/2\beta}$ elimination half-life, *MRT* mean residence time. **c** The saturation assay of ^{131}I-A8. K_D equilibrium dissociation constant, B_{max} maximum number of binding sites. **d** The competition binding assay of ^{131}I-A8. K_i inhibitor constant, IC_{50} half maximal inhibitory concentration

were treated with different concentrations of A8 (0, 5, 10, 20, 40, and 60 μg/ml), and A8 markedly suppressed cell growth in time-dependent and dose-dependent manner. The proliferation inhibition ratio of the A8 (20 μg/ml) group (17.6±1.23 %, 32.2.6±1.06 %, and 39.9±0.96 % at 24, 48, and 72 h, respectively) was significantly higher than that of the A8 (5 μg/ml) group (4.9±1.24 %, 6.9±0.95 %, 7.2±1.52 %) (P<0.01) (Fig. 1b). This antiproliferative role for A8 was also

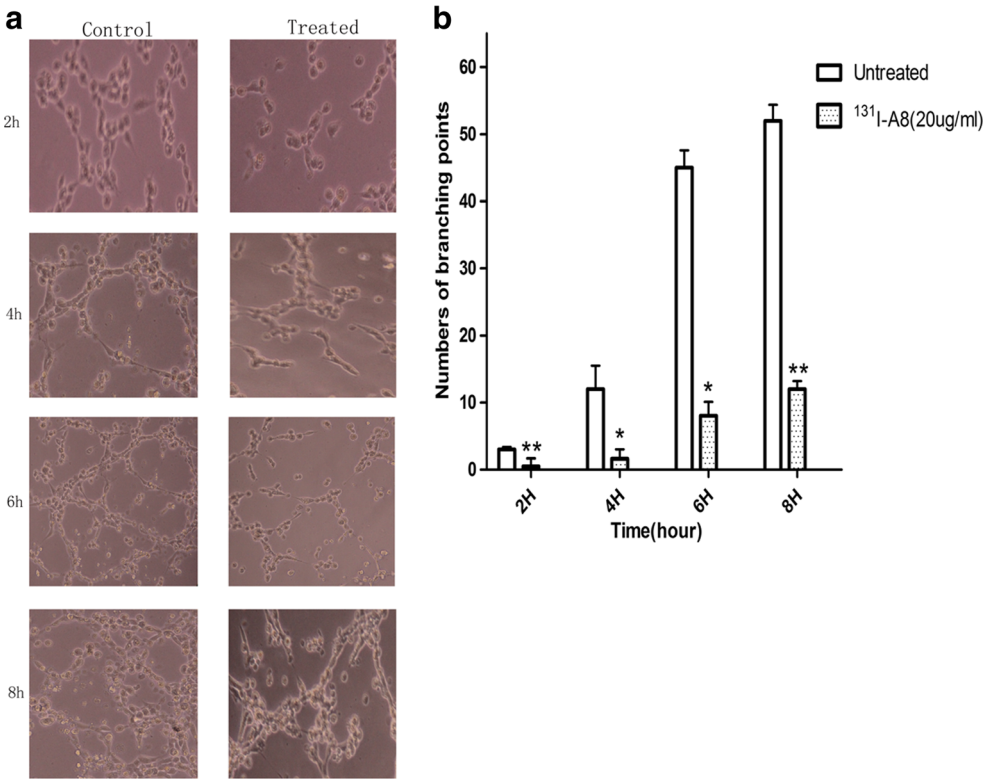

Fig. 3 The tube formation inhibition of ^{131}I-A8 was detected in HUVECs angiogenesis model. **a** Representative photographs of each treatment were shown (100×). **b** The total numbers of branching points were decreased compared with the untreated (*P<0.05 and **P<0.01 vs. control)

presented in the HUVECs, and increased concentrations of A8 between 0 and 60 μg/ml lead to increased inhibition of HUVECs growth. The highest proliferation inhibition ratio in this experiment was up to 45.2±1.26 % when incubated with A8 (60 μg/ml) for 72 h. Collectively, these results demonstrated that treatment of SMMC7721-GFP cells and HUVECs with A8 exhibited a time-dependent and dose-dependent manner suppression of both two cell lines proliferation.

The synthesis and pharmacokinetic analysis

^{131}I-A8 was radioiodinated using the iodogen technique. The radiolabeling efficiency was 97.4 %. The radiochemical purity of ^{131}I-A8 was 92.8 %. The specific activity of radioiodinated A8 is 69.7±6.26 MBq/μmol. For in vitro stability test, the radiochemical purities of ^{131}I-A8 were still over 90 % in serum and declined under 80 % in saline at 72 h, indicating that they maintained more stable in serum than in saline. These results showed that ^{131}I-A8 had good stability (Fig. 2a). Pharmacokinetic analysis showed that the pharmacokinetics of ^{131}I-A8 was in accordance with the two-compartment model, with a rapid distribution phase and a slow decline phase. $T_{1/2\alpha}$, $T_{1/2\beta}$, and MRT were 7.1, 144.5, and 10 h, respectively. (Fig. 2b).

The affinity of ^{131}I-A8 against SMMC7721-GFP cells

Radioligand-based binding assay is a sensitive technique available to quantitatively determine the affinity of one antibody against a certain receptor. Saturation assay showed that ^{131}I-A8 displayed saturable binding with SMMC7721-GFP cells and K_D and B_{max} were 3.99±0.64 nM and 142,874±456 cpm respectively (Fig. 2c). The unlabeled A8 competed effectively with ^{131}I-A8 binding sites on SMMC7721-GFP cells at low micromole concentrations, and K_i and IC_{50} were 8.81±1.02 and 30.85±1.33 nM, respectively (Fig. 2d). All of above demonstrated that high affinity of ^{131}I-A8 against SMMC7721-GFP cells.

Tube formation assay

A HUVECs angiogenesis model was employed to evaluate the capacity of tube formation of HUVECs. As illustrated in Fig. 3a, HUVECs which were treated with 20 μg/ml ^{131}I-A8 were effectively inhibited to form extensive and enclosed tube networks as compared with the untreated ones. Furthermore, the formation time of vascular like structures was significantly delayed in the ^{131}I-A8-treated group than the untreated group (data was not shown).

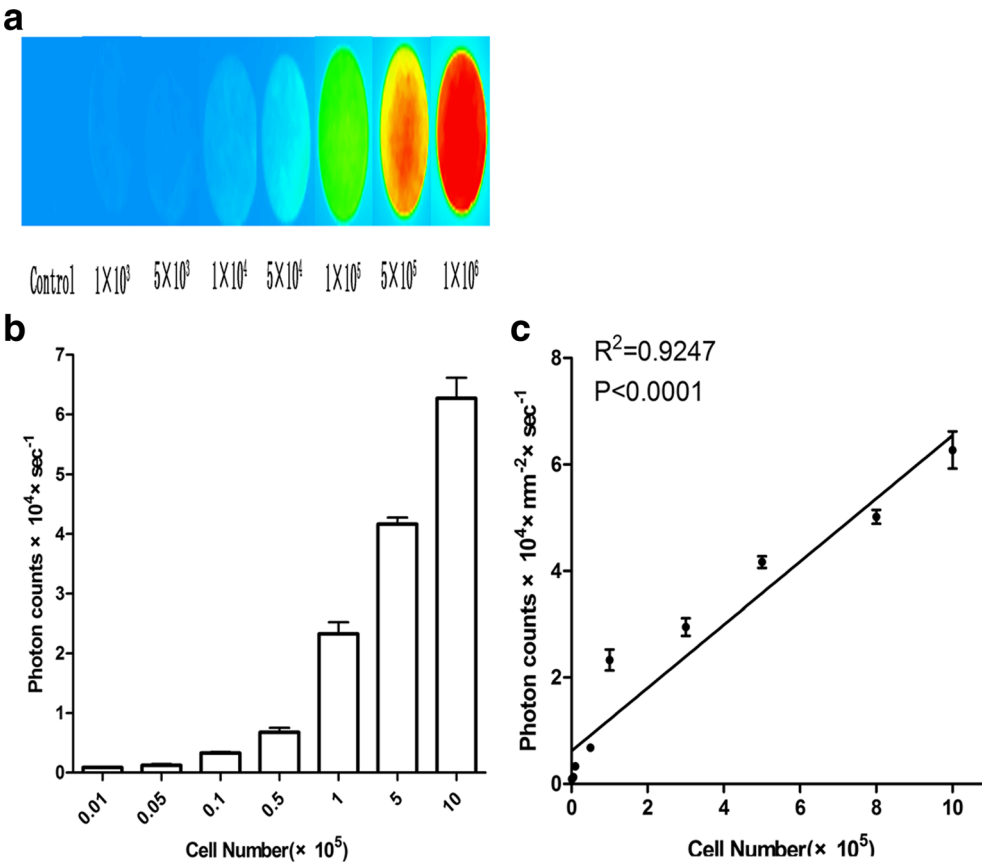

Fig. 4 Quantification of the SMMC7721-GFP cells number and fluorescent signals in vitro. **a**–**b** Each cell aliquot was assessed by measuring intensity in vitro with NIFLI. Data are plotted as net photon counts (summary background) with standard deviation. **c** In vitro fluorescent signal is strongly correlated to cell number over a broad dynamic range. Control: PBS

NIFLI

In vitro fluorescent signal is strongly correlated to cell number over a broad dynamic range (r^2=0.9247, P<0.01) (Fig. 4a–c). SMMC7721-GFP cells (5×10^6) were injected into the right upper back of nude mice to monitor subcutaneous tumor growth by caliper measurement and NIFLI. Tumor growth was measured beginning on day 5 after injection and three times per week thereafter. All mice showed successful tumor development on d5 by NIFLI and caliper measurements. Overall, fluorescent signal and tumor volume were highly correlative (r^2=0.925, P<0.01) (Fig. 5a–d).

Tumor prevention study and therapeutic evaluation

To evaluate the capacities of NIFLI for monitoring the tumor burden in a therapeutic setting, ^{131}I-A8 treatment was administered intratumorally once a week for a month when tumor volume increased to 50 mm^3. The imaging data shows a continuous increasing fluorescent signals in the control group of PBS-treated mice, whereas a significant reduction in tumor burden was seen in the mice treated with ^{131}I-A8 ($^{*}P$<0.05 and $^{**}P$<0.01 vs. control) (Fig. 6b). Figure 6c–d shows the course of the fluorescent signals for one representative mouse in the control and ^{131}I-A8 therapy groups. Again, photon counts and tumor volume were highly correlative (r^2=0.947, P<0.01). After 4 weeks of ^{131}I-A8 treatment, tumor weight was significantly decreased in ^{131}I-A8-treated group compared with PBS-treated group (Fig. 6f, g) (P<0.01), and the inhibition rate was 62.1 %. Collectively, these results suggest that ^{131}I-A8 treatment is significantly effective in reducing tumor growth in an HCC mouse model.

ENG mRNA and protein expression

ENG protein expression was assessed by immunohistochemistry staining. ENG protein was mainly localized to cell membranes (Fig. 7a). ENG protein level was significantly higher in HCC tissue in PBS-treated mice than that in normal liver tissue (**P<0.01 vs. control). Compared with the PBS treated mice, there was significantly lower ENG protein level in ^{131}I-A8-treated mice (#P<0.01 vs. tumor 2) (Fig. 7b). ENG mRNA expression was quantified by RT-PCR. ENG expression in the SMMC7721-GFP group was markedly higher than that in the normal liver cell L-02 group. Between the two groups, there was a significant difference (P<0.01). Similarly, there was a significantly higher ENG mRNA level in HCC tissue than that in normal liver tissue (Fig. 7c, d).

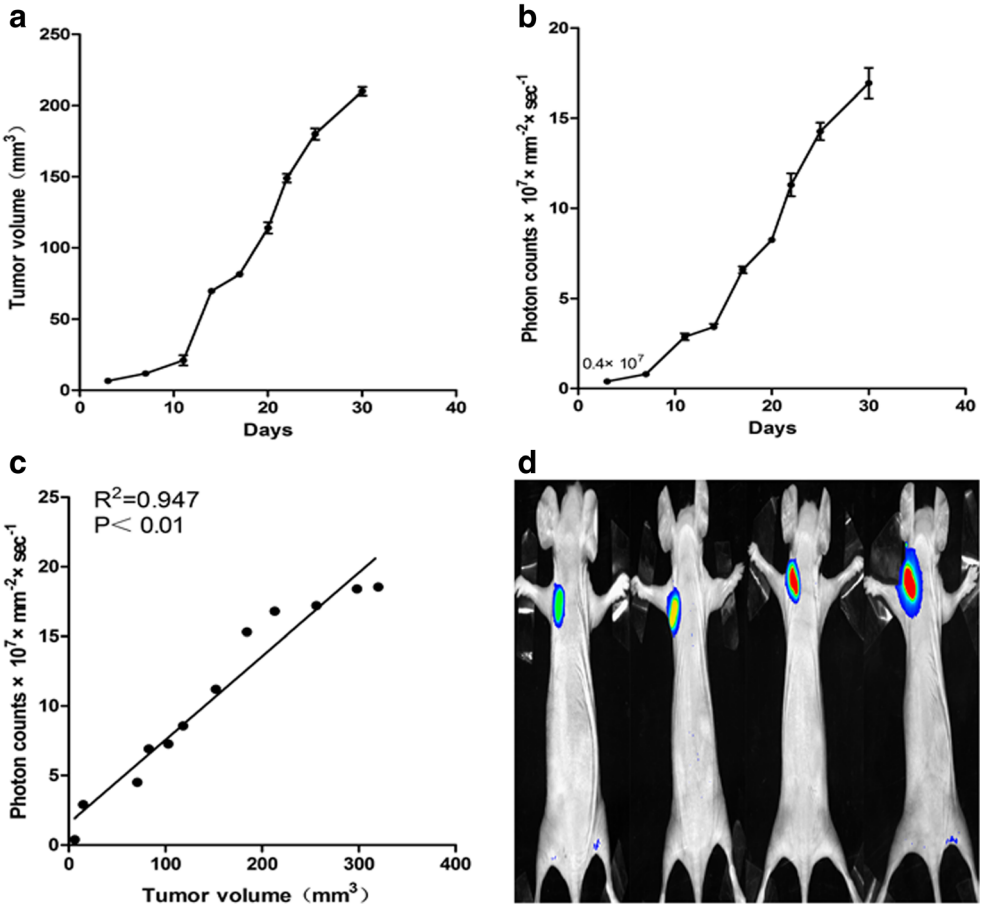

Fig. 5 Quantification of tumor volume and fluorescent signals over time of subcutaneous tumor growth. **a** Tumor volume over time (n=8 animals). Tumor volume was calculated using the following formula: volume=(length×width^2)/2; tumor size was measured by calipers. **b** Quantification of the fluorescent signal over time. **c** Correlation between mean tumor volume and mean fluorescent signal. **d** One representative animal shows the increase of fluorescent signal and tumor volume over time

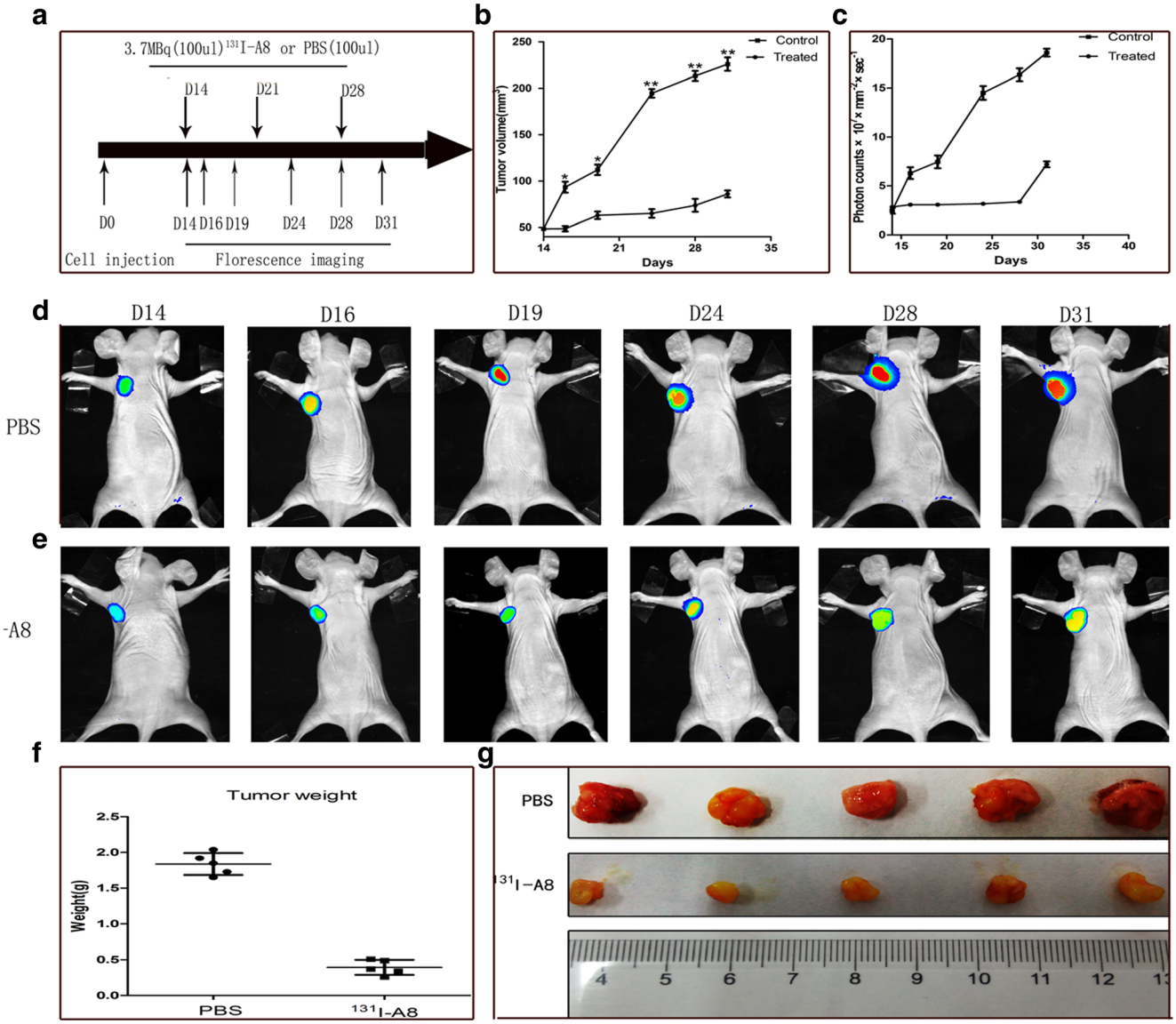

Fig. 6 Monitoring ^{131}I-A8 radioimmunotherapy efficacies on tumor growth. **a** The scheme described the time points when ^{131}I-A8 was injected and NIFLI was conducted. **b** When the tumor volume was up to 50 mm^3, mice were treated intratumorally with injections of ^{131}I-A8 once a week for a month. Average size of the tumors of mice during treatment with ^{131}I-A8 or control PBS (n=8 in each group). There is a significant difference in tumor size between the two groups (*P<0.05 and **P<0.01 vs. control). **c** Quantification of the fluorescent signal over time for the two groups. **d**–**e** Representative NIFLI images during tracking tumor growth. **f** Decreased excised tumor weights of ^{131}I-A8-treated mice compared to PBS treated at the day of 31 (P<0.01 treated compared to PBS). Results are shown as mean SD of eight individual animals. **g** Representative tumor images from different groups at the day of 31

Discussion

HCC is the fifth most common cancer worldwide, and its incidence is very high in China where it is the second most common cancer. Because many patients are at increased risk of HCC, there is a need to develop reliable, sensitive, and specific markers that will aid the clinician in early diagnosis and therapy [24, 25]. HCC tumors depend on a rich blood supply [26, 27]; therefore, inhibition of angiogenesis has constituted a crucial point in liver cancer therapy.

Tumor angiogenesis has been considered to be an attractive target for therapeutic strategies for many decades. Among antibodies with antiangiogenetic activity so far tested in cancer patients, only the humanized anti-VEGF mAb bevacizumab has received approval by regulatory agencies, though for selected clinical indications [28, 29]. However, the effectiveness of anti-VEGF therapy in the clinic proved to be strongly tumor-type-dependent, and effects were mostly transient, due to resistance. Therefore, these therapies did not meet the high expectations of increasing patient survival in many tumor types and even

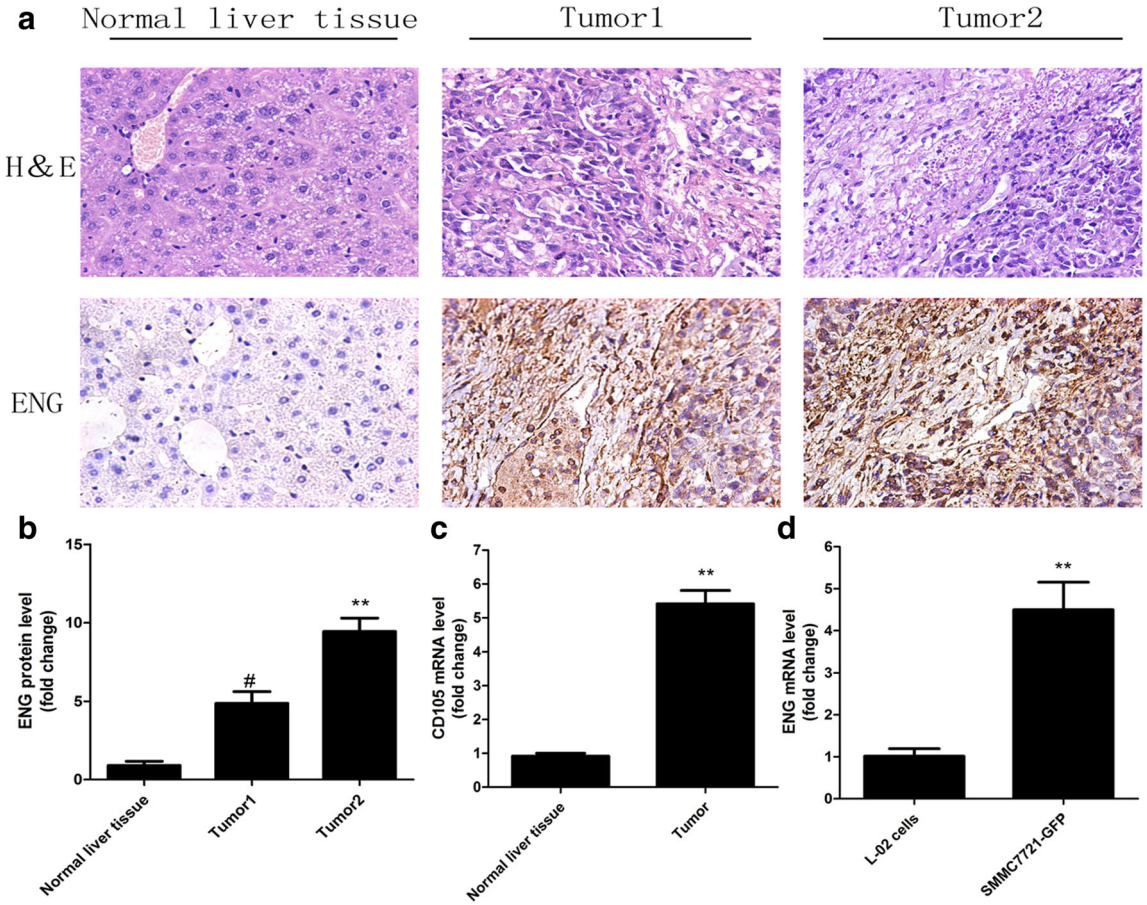

Fig. 7 ENG mRNA and protein expression. **a** Representative hematoxylin and eosin staining (H&E) and immunohistochemical staining for ENG protein (original magnification ×200), normal liver tissue (control); tumor of ^{131}I-A8-treated mouse (tumor 1); tumor of PBS-treated mouse (tumor 2). **b** Quantification of ENG protein levels in immunohistochemical staining (**P<0.01 vs. control. #P<0.01 vs. tumor 2). **c**–**d** Relative mRNA expression of ENG in SMMC7721-GFP, L-02, normal liver tissue (control), and hepatocellular carcinoma tissue (**P<0.01 vs. control). Fold changes represent the mean of triplicate experiments compared to untreated control group. A pattern of results was analyzed by repeating at least three times. *Columns* represent the mean; *bars* represent SD

led to the withdrawal of FDA approval for anti-VEGF therapy in breast cancer [30]. One of the major mechanisms of resistance to anti-VEGF therapy is the upregulation of alternative proangiogenic pathways [31], opening the possibility to explore these pathways to serve as novel antiangiogenesis targets.

ENG is a TGF-β coreceptor that modulates TGF-β-dependent cellular responses. Several reports indicate an indispensable role for the TGF-β signaling pathway in developmental angiogenesis. ENG in developmental angiogenesis was first demonstrated by the death of ENG knockout mice due to vascular development defects, particularly of the primitive vascular plexus of the yolk sac, by gestational day 11.5 [32]. In addition, mutations in the ENG gene have been described in human. It is generally accepted that ENG haploinsufficiency results in the autosomal dominant syndrome hereditary hemorrhagic telangiectasia type 1(HHT1) [33]. Many studies have defined the role of ENG as a powerful marker to quantify intratumoral microvessel density (IMVD) in solid and hematopoietic tumors such as breast [34], prostate [35], cervical [36], colorectal [37], nonsmall cell lung cancer (NSCLC) [38], HCC, and in multiple myeloma [39]. Recently, ENG has been reported to play a role in the regulation of adhesion, motility, and invasion of several kinds of human cancer cells [40]. Furthermore, considerable efforts based on ENG have been made recently in the early detecting of tumors, and radiolabeled anti-ENG mAb efficiently imaged human melanoma xenografts in C57BL/6 mice [41] and spontaneous mammary adenocarcinomas in a canine model [42]. In this setting, targeting of ENG is generally considered a promising therapeutic strategy to control tumor angiogenesis.

In the present study, we found that anti-ENG mAb can effectively inhibit the proliferation of SMMC7721-GFP, the proliferation inhibition ratio up to 39.9±0.96 % after incubated with anti-ENG mAb (60 μg/ml) for 72 h. Furthermore, the proliferation of HUVECs was also significantly restrained by anti-ENG mAb, and the formation of the tube networks was prevented in vitro. These findings are consistent with previous observations that anti-ENG antibodies can inhibit proliferation, migration, and adhesion of endothelial cells [43]. Based

on our results, we consider that the probable mechanism of the tumor suppression of anti-ENG mAb is to direct inhibition of HCC growth, restrain the formation of the tube, and block the blood supply for the tumor further.

Molecular imaging, which allows for sensitive, longitudinal observation, has become an invaluable tool for early lesion detection, monitoring therapeutic efficacy, and facilitating drug development [15]. In recent years, optical molecular imaging has emerged as an important tool of technologies to advance our understanding of disease mechanisms and accelerate drug discovery [44]. NIFLI technique is a sensitive and fast in vivo cellular and molecular imaging method, allowing use of cells transfected with fluorescent gene or specific molecular probes and sensitive fluorescent imaging system to perform real-time, noninvasive, dynamic, and in vivo observation and analysis on different gene expressions, cell surface protein markers, and diseased cells. In this study, we use an HCC cell line SMMC7721 which stably expressed GFP and shows a good correlation between the fluorescent signal and the number of cancer cells in vitro. Meanwhile, we also demonstrated a good correlation between the fluorescent signal and tumor size in a subcutaneous hepatoma model with SMMC7721-GFP cells. Therefore, we can be noninvasive, accurate, and capable of continuously monitoring the therapy of tumor by fluorescent imaging. Combination of tumor vessel-targeted therapy with other therapies such as immunotherapy and radiotherapy may enhance therapeutic efficacy compared with either therapy alone [45]. ^{131}I is a widely used therapeutic radionuclide in clinical practice [46]. It has been easy labeling and is inexpensive, with a half-life of 8 days [47]. In the present study, ^{131}I-A8 was successfully radioiodinated and was proved to have high affinity against ENGR. Following subcutaneous injection of SMMC7721-GFP cells, mice treated with ^{131}I-A8 exhibited significant tumor suppression compared with that of PBS group. Considering the therapeutic results in this study, we were able to demonstrate that significant antitumor effect of ^{131}I-A8 in HCC on the basis of a significantly reduced fluorescence signal by NIFLI and a remarkably decreased tumor weight in treated animals. The result is in accordance with previous studies demonstrating a long-lasting regression/suppression of tumor growth and metastasis in mice by the anti-ENG mAb [48].

In conclusion, our study indicated that ENG could be a promising candidate for molecular-targeted therapy for HCC. Furthermore, NIFLI can be used to monitor the therapeutic effect of tumor burden mice based on the good relationship between the fluorescence imaging and tumor volume.

Acknowledgments This study was supported by the Natural Science Foundation of Shandong Province (No. Y2007C088), the China Postdoctoral Science Foundation (No. 20090461227), and the Science and Technology Project of Shandong, China (2013GSF11843).

Conflicts of interest None

References

1. Gramantieri L, Fornari F, Callegari E, Sabbioni S, Lanza G, Croce CM, et al. MicroRNA involvement in hepatocellular carcinoma. J Cell Mol Med. 2008;12:2189–204.
2. Forner A, Reig M, Bruix J. Alpha-fetoprotein for hepatocellular carcinoma diagnosis: the demise of a brilliant star. Gastroenterology. 2009;137:26–9.
3. Cabrera R, Nelson DR. Review article: the management of hepatocellular carcinoma. Aliment Pharmacol Ther. 2010;31:461–76.
4. Moribe T, Iizuka N, Miura T, Kimura N, Tamatsukuri S, Ishitsuka H, et al. Methylation of multiple genes as molecular markers for diagnosis of a small, well-differentiated hepatocellular carcinoma. Int J Cancer. 2009;125:388–97.
5. Marrero JA, Welling T. Modern diagnosis and management of hepatocellular carcinoma. Clin Liver Dis. 2009;13:233–47.
6. Bruix J, Sherman M. Management of hepatocellular carcinoma. Hepatology. 2005;42:1208–36.
7. Llovet JM, Burroughs A, Bruix J. Hepatocellular carcinoma. Lancet. 2003;362:1907–17.
8. Beecken WD, Kramer W, Jonas D. New molecular mediators in tumor angiogenesis. J Cell Mol Med. 2000;4:262–9.
9. Fonsatti E, Del Vecchio L, Altomonte M, Sigalotti L, Nicotra MR, Coral S, et al. Endoglin: an accessory component of the TGF-β-binding receptor-complex with diagnostic, prognostic, and bioimmunotherapeutic potential in human malignancies. J Cell Physiol. 2001;188:1–7.
10. Miller DW, Graulich W, Karges B, Stahl S, Ernst M, Ramaswamy A, et al. Elevated expression of endoglin, a component of the TGF-β-receptor complex, correlates with proliferation of tumor endothelial cells. Int J Cancer. 1999;81:568–72.
11. Derynck R, Zhang YE. Smad-dependent and Smad-independent pathways in TGF-beta family signalling. Nature. 2003;425:577–84.
12. Zavadil J, Bottinger EP. TGF-beta and epithelial-to-mesenchymal transitions. Oncogene. 2005;24:5764–74.
13. Yang LY, Lu WQ, Huang GW, Wang W. Correlation between CD105 expression and postoperative recurrence and metastasis of hepatocellular carcinoma. BMC Cancer. 2006;6:110.
14. Chen HJ, Yang BL, Chen YG, Lin Q, Zhang SP, Gu YF. A GFP-labeled human colon cancer metastasis model featuring surgical orthotopic implantation. Asian Pac J Cancer Prev. 2012;13:4263–6.
15. Zhang Q, Du Y, Xue Z, Chi C, Jia X, Tian J. Comprehensive evaluation of the anti-angiogenic and anti-neoplastic effects of endostar on liver cancer through optical molecular imaging. Plose One. 2014;9:e 85559. doi:10.1371/journal.pone.0085559.
16. Zhang C, Hou G, Liang T, Song J, Qu L, et al. A prospective study of macrophage migration inhibitory factor as a marker of inflammatory detection. J Cell Mol Med. 2009;13:4077–83.
17. Hao PP, Liu YP, Yang CY, Liang T, Zhang C, Song J, et al. Evaluation of ^{131}I-anti-angiotensin II type 1 receptor monoclonal antibody as a reporter for hepatocellular carcinoma. Plose One. 2014;9:e85002. doi:10.1371/journal.pone.0085002.
18. Bonde MM, Hansen JT, Sanni SJ, Haunsø S, Gammeltoft S, Lyngsø C, et al. Biased signaling of the angiotensin II type 1 receptor can be mediated through distinct mechanisms. Plose One. 2010;5:e14135. doi:10.1371/journal.pone.0014135.
19. Wu C, Wei J, Tian D, Feng Y, Miller RH, Wang Y. Molecular probes for imaging myelinated white matter in CNS. J Med Chem. 2008;51:6682–8.

20. Rhim JS, Tsai WP, Chen ZQ, Chen Z, Van Waes C, Burger AM, et al. A human vascular endothelial cell model to study angiogenesis and tumorigenesis. Carcinogenesis. 1998;19:673–81.
21. Clarke K, Lee FT, Brechbiel MW, Smyth FE, Old LJ, Scott AM. In vivo biodistribution of a humanized anti-Lewis Y monoclonal antibody (hu3S193) in MCF-7 xenografted BALB/c nude mice. Cancer Res. 2000;60:4804–11.
22. Huynh H, Chow KH, Soo KC, Toh HC, Choo SP, Foo KF, et al. RAD001 (everolimus) inhibits tumour growth in xenograft models of human hepatocellular carcinoma. J Cell Mol Med. 2009;13:1371–80.
23. He L, Zhou X, Qu C, Hu L, Tang Y, Zhang Q, et al. Musashi2 predicts poor prognosis and invasion inhepatocellular carcinoma bydriving epithelial-mesenchymal transitio. J Cell Mol Med. 2014;18:49–58.
24. Seon BK, Matsuno F, Haruta Y, Kondo M, Barcos M. Long-lasting complete inhibition of human solid tumors in SCID mice by targeting endothelial cells of tumor vasculature with antihuman endoglin immunotoxin. Clin Cancer Res. 1997;3:1031–44.
25. Semela D, Dufour JF. Angiogenesis and hepatocellular carcinoma. J Hepatol. 2004;41:864–80.
26. Tam K. The roles of doxorubicin in hepatocellular carcinoma. ADMET DMPK. 2013;1:29–44.
27. Ferrara N. VEGF as a therapeutic target in cancer. Oncology. 2005;69:11–6.
28. Ferrara N, Kerbel RS. Angiogenesis as a therapeutic target. Nature. 2005;438:967–74.
29. Sitohy B, Nagy JA, Dvorak HF. Anti-VEGF/VEGFR therapy for cancer: reassessing the target. Cancer Res. 2012;72:1909–14.
30. Bergers G, Hanahan D. Modes of resistance to anti-angiogenic therapy. Nat Rev Cancer. 2008;8:592–603.
31. Li DY, Sorensen LK, Brooke BS, Urness LD, Davis EC, Taylor DG, et al. Defective angiogenesis in mice lacking endoglin. Science. 1999;284:1534–7.
32. McAllister KA, Baldwin MA, Thukkani AK, Gallione CJ, Berg JN, Porteous ME, et al. Six novel mutations in the endoglin gene in hereditary hemorrhagic telangiectasia type 1 suggest a dominant-negative effect of receptor function. Hum Mol Genet. 1995;4:1983–5.
33. Kumar S, Ghellal A, Li C, Byrne G, Haboubi N, Wang JM, et al. Breast carcinoma vascular density determined using CD105 antibody correlates with tumor prognosis. Cancer Res. 1999;59:856–61.
34. Wikström P, Lissbrant IF, Stattin P, Egevad L, Bergh A. Endoglin (CD105) is expressed on immature blood vessels and is a marker for survival in prostate cancer. Prostate. 2002;51:268–75.
35. Brewer CA, Setterdahl JJ, Li MJ, Johnston JM, Mann JL, McAsey ME. Endoglin expression as a measure of microvessel density in cervical cancer. Obstet Gynecol. 2000;96:224–8.
36. Akagi K, Ikeda Y, Sumiyoshi Y, Kimura Y, Kinoshita J, Miyazaki M, et al. Estimation of angiogenesis with anti-CD105 immunostaining in the process of colorectal cancer development. Surgery. 2002;131: S109–13.
37. Tanaka F, Otake Y, Yanagihara K, Kawano Y, Miyahara R, Li M, et al. Evaluation of angiogenesis in non-small cell lung cancer: comparison between anti-CD34 antibody and anti-CD105 antibody. Clin Cancer Res. 2001;7:3410–5.
38. Pruneri G, Ponzoni M, Ferreri AJ, Decarli N, Tresoldi M, Raggi F, et al. Microvessel density, a surrogate marker of angiogenesis, is significantly related to survival in multiple myeloma patients. Br J Haematol. 2002;118:817–20.
39. Liu Y, Jovanovic B, Pins M, Lee C, Bergan RC. Over expression of endoglin in human prostate cancer suppresses cell detachment, migration and invasion. Oncogene. 2002;21:8272–81.
40. Bredow S, Lewin M, Hofmann B, Marecos E, Weissleder R. Imaging of tumour neovasculature by targeting the TGF-beta binding receptor endoglin. Eur J Cancer. 2000;36:675–81.
41. Dallas NA, Samuel S, Xia L, Fan F, Gray MJ, Lim SJ, et al. Endoglin (CD105): a marker of tumor vasculature and potential target for therapy. Clin Cancer Res. 2008;14:1931–7.
42. She X, Matsuno F, Harada N, Tsai H, Seon BK. Synergy between anti-endoglin(CD105) monoclonal antibodies and TGF-beta in suppression of growth of human endothelial cells. Int J Cancer. 2004;108:251–7.
43. Jaffer FA, Libby P, Weissleder R. Optical and multimodality molecular imaging: insights into atherosclerosis. Arterioscler Thromb Vasc Biol. 2009;29:1017–24.
44. Gasparini G, Longo R, Fanelli M, Teicher BA. Combination of antiangiogenic therapy with other anticancer therapies: results, challenges, and open questions. J Clin Oncol. 2005;23: 1295–311.
45. Barnard A, Smith DK. Self-assembled multivalency: dynamic ligand arrays for high-affinity binding. Angew Chem Int Ed Engl. 2012;51: 6572–81.
46. Hu H, Liu J, Yao L, Yin J, Su N, Liu X, et al. Real-time bioluminescence and tomographic imaging of gastric cancer in a novel orthotopic mouse model. Oncol Rep. 2012;27:1937–43.
47. Tsujie M, Tsujie T, Toi H, Uneda S, Shiozaki K, Tsai H, et al. Anti-tumor activity of an anti-endoglin monoclonal antibody is enhanced in immunocompetent mice. Int J Cancer. 2008;122: 2266–73.
48. Uneda S, Toi H, Tsujie T, Tsujie M, Harada N, Tsai H, et al. Anti-endoglin monoclonal antibodies are effective for suppressing metastasis and the primary tumors by targeting tumor vasculature. Int J Cancer. 2009;125:1446–53.